ETHzürich

Aptamer Conformational Change Enables Serotonin Biosensing with Nanopipettes

Journal Article

Author(s):
Nakatsuka, Nako (iD); Faillétaz, Alix; Eggemann, Dominic; Forró, Csaba; Vörös, Janos (iD); Momotenko, Dmitry

Aptamer Conformational Change Enables Serotonin Biosensing with Nanopipettes

Journal:	*Analytical Chemistry*
Manuscript ID	ac-2020-05038b.R1
Manuscript Type:	Article
Date Submitted by the Author:	27-Jan-2021
Complete List of Authors:	Nakatsuka, Nako; ETH Zürich, Department of Information Technology and Electrical Engineering Faillétaz, Alix; Eidgenossische Technische Hochschule Zurich, Laboratory of Biosensors and Bioelectronics Eggemann, Dominic; Eidgenossische Technische Hochschule Zurich, Laboratory of Biosensors and Bioelectronics Forró, Csaba; Eidgenossische Technische Hochschule Zurich Vörös, Janos; Eidgenossische Technische Hochschule Zurich, Laboratory of Biosensors and Bioelectronics Momotenko, Dmitry; ETH-Zurich, Institute for Biomedical Engineering

SCHOLARONE™
Manuscripts

Aptamer Conformational Change Enables Serotonin Biosensing with Nanopipettes

Nako Nakatsuka, Alix Faillétaz, Dominic Eggemann, Csaba Forró,[†] János Vörös,[*] and Dmitry Momotenko[*]

*To whom correspondence should be addressed: janos.voros@biomed.ee.ethz.ch and momotenko@biomed.ee.ethz.ch

Laboratory of Biosensors and Bioelectronics, Institute for Biomedical Engineering, ETH Zürich, CH-8092, Switzerland

ABSTRACT: We report artificial nanopores in the form of quartz nanopipettes with *ca.* 10 nm orifices functionalized with molecular recognition elements termed aptamers that reversibly recognize serotonin with high specificity and selectivity. Nanoscale confinement of ion fluxes, analyte-specific aptamer conformational changes, and related surface charge variations enable serotonin sensing. We demonstrate detection of physiologically relevant serotonin amounts in complex environments such as neurobasal media in which neurons are cultured *in vitro*. In addition to sensing in physiologically relevant matrices with high sensitivity (picomolar detection limits), we interrogate the detection mechanism *via* complementary techniques such as quartz crystal microbalance with dissipation monitoring and electrochemical impedance spectroscopy. Moreover, we provide a novel theoretical model for structure-switching aptamer-modified nanopipette systems that supports experimental findings. Validation of specific and selective small-molecule detection in parallel with mechanistic investigations, demonstrates the potential of conformationally changing aptamer-modified nanopipettes as rapid, label-free, and translatable nanotools for diverse biological systems.

INTRODUCTION

Measuring specific chemical interactions at the spatiotemporal resolution that approaches biologically meaningful dimensions and timescales is critical to understand neuronal communication. Various studies have shown that neurotransmitter receptors play critical roles in the process of learning and adaptation, *i.e.* plasticity implemented at synapses.[1–3] In particular, dysfunction in synaptic signaling mediated by serotonin, a modulator of essential brain functions such as cognitive control, sensory processing, and emotional regulation, has been linked to neuronal network defects that lead to neurodevelopmental and subsequent psychiatric disorders.[4,5] However, existing methods of serotonin sensing capable of resolving local biomolecular responses in close proximity to synapses (*ca.* 20 nm space) are scarce and experimentally challenging.

While the gold standard for serotonin quantification is microdialysis sampling coupled to high performance liquid chromatography or mass spectrometry, the spatiotemporal resolution is insufficient to reveal the dynamics in complex neuronal circuits.[6–8] Alternatively, electrochemical sensing methods such as fast-scan cyclic voltammetry, which have the required temporal resolution to measure rapid neurotransmitter dynamics,[9-11] face selectivity issues as many neurochemicals have the same electroactive moiety with overlapping redox potentials.[12,13] Further, despite advances in surface modification strategies,[14] microelectrodes are vulnerable to fouling due to the strong adsorption of the serotonin oxidation product.[15] In lieu of implantable electrodes, optical platforms have been developed for detecting serotonin, albeit with issues such as low binding
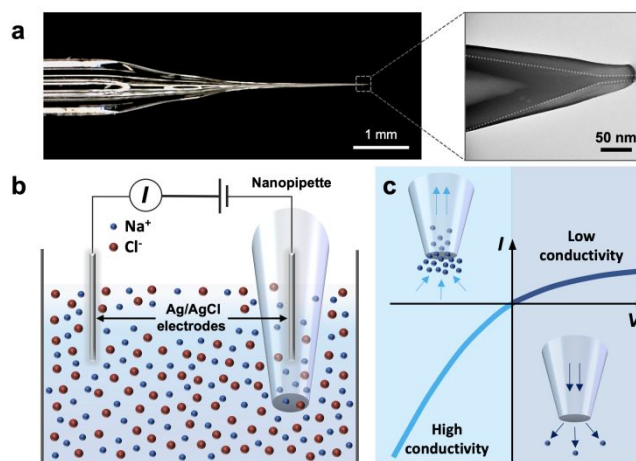

Figure 1. Aptamer-modified nanopipette sensing principle. (**a**) Optical microscope image of a nanopipette (left) with a magnified transmission electron microscopy, TEM, image (right) that demonstrates the approximate pore opening of *ca.* 10 nm. The dotted line is drawn to aid visualization of the inner wall at the tip of the nanopipette. (**b**) The schematic of a nanopipette voltammetry setup comprising a quartz pipette with an Ag/AgCl quasi-reference counter electrode inserted inside while another Ag/AgCl quasi-reference is placed in the bulk solution to apply electrical bias to the system. The nanopipettes are filled with phosphate buffered saline (PBS), the same buffer as the bulk solution. (**c**) Schematic describing the ion current rectification effect. The geometry and surface charges at the nanopipette tip induce an accumulation or depletion of cations (anions are not depicted) when a negative or positive bias is applied respectively, which influences the conductivity through the pore in a nonlinear manner.

1

affinities, cross-reactivity, and with highly specialized instrumentation.[16,17]

Besides the need for detecting neurotransmitters *in vivo* there is also an emerging community that attempts to learn about neural networks *in vitro*. This bottom-up neuroscience approach uses well-defined cultured neuronal networks to investigate basic neural circuits with the hope to gain insight into information processing, storage, and neurocomputation in the brain.[18,19]

Novel nanotools with dimensions comparable to synapses with high chemical selectivity and sensitivity would be highly useful for both neuroscience approaches.[20] Nanopore-based sensing systems hold great promise for such measurements, where intermolecular interactions are confined to nanoscale volumes, therefore enabling molecular identification at the single-molecule level.[21-25] However, the low spatial resolution due to static sensing areas, prevents their applicability for sensing from living cells. Recently, this challenge was tackled by a force-controlled scanning nanopore microscope system based on positioning of mobile nanopores fabricated on cantilevers in close proximity of living cells.[26] While powerful, this approach currently exhibits low selectivity, which needs to be addressed to enable differentiation of small-molecule neurotransmitters.[12]

Herein, we tackle the aforementioned issues by using chemically functionalized mobile quartz nanopipettes with pore openings of *ca.* 10 nm (Figure 1a). These solid-state nanopores are promising candidates for small-molecule sensing due to the capacity to tune their opening size down to a few nanometers, straightforward fabrication and surface modification, and ease of coupling to scanning probe methodologies[27–29] to interface with biological systems. The ion current induced by an applied voltage is measured between two electrodes in solutions separated by a nanopore of the pipette (Figure 1b). In conically-shaped nanopipettes with pore diameters of comparable size to the electrical double layer, the ion-current rectification (ICR) effect is observed.[30–32] This phenomenon introduces asymmetric flux of ions through the nanopore whereby nanopipettes respond to a symmetric applied voltage sweep with a nonlinear asymmetric current output, deviating from ohmic behavior (Figure 1c).[33] For quartz nanopipettes, the combination of the applied voltage, nanopore geometry, and surface charges result in a difference in ion transport rates inside and outside the nanopore that lead to accumulation or depletion of charge carriers.[34–36]

EXPERIMENTAL METHODS

Materials. All chemicals were purchased from Sigma-Aldrich Chemie GmbH (Buchs, Switzerland) unless otherwise noted below. Phosphate buffer saline at 1x concentration (137 mM NaCl, 2.7 mM KCl, 10 mM Na_2HPO_4, 1.8 mM KH_2PO_4) and pH 7.4 (ThermoFisher Scientific AG, Reinach, Switzerland) was used as received for all measurements. All solutions were prepared using deionized water with resistivity 18.2 MΩ cm^{-1} produced by a Milli-Q system (Millipore, Billerica, MA). Neurobasal medium™ (NBM) was supplemented with 2% B27, 1% GlutaMAX, and 1% penicillin streptomycin (all from ThermoFisher Scientific AG, Reinach, Switzerland).

Thiolated single-stranded serotonin aptamer: (5'/Thiol/-CGA CTG GTA GGC AGA TAG GGG AAG CTG ATT CGA TGC GTG GGT CG-3') with molecular weight 13,969.8 g/mol, melting point 74 °C, and thiolated scrambled

sequence: (5'/Thiol/-CCC GGG AAT TCC GGA ATT GGG GCA AATT GAT GAG GGG GTC ATG GG-3') with molecular weight 13,969.8 g/mol, melting point 71.4 °C, were purchased from Microsynth AG (Balgach, Switzerland). All DNA solutions (100 μM) were HPLC purified, aliquoted, and stored at -20 °C until use. The scrambled sequence was designed by modeling *via* MFold[37] to ensure that there is a significant difference in the secondary structure *versus* the target-specific sequence.

Nanopipette fabrication and characterization. Nanopipettes were pulled from quartz capillaries (o.d., 1 mm; i.d., 0.5 mm; Friedrich & Dimmock) using a laser puller (P2000, Sutter Instruments). The pulling parameters for the nanopipettes with apertures ~10 nm were: (line 1) Heat 750, Filament 4, Velocity 40, Delay 150, and Pull 80; (line 2) Heat 700, Filament 3, Velocity 60, Delay 135, Pull 180. The pulling parameters for the ~20 nm opening pipettes were: (line 1) Heat 750, Filament 4, Velocity 40, Delay 150, and Pull 80; (line 2) Heat 700, Filament 3, Velocity 50, Delay 135, Pull 150. The laser puller was heated at least 1 h before use. Dimensions of the individual nanopipettes used in experiments in this work were measured *via* transmission electron microscopy (TEM) using Jeol JEM-1400 at 200 kV accelerating voltage.

Aptamer functionalization. DNA aptamers were immobilized on the inside of the nanopipette tip *via* a three-step functionalization procedure.[38] First, (3-aminopropyl)trimethoxysilane (APTMS) was deposited on the nanopipette surfaces using vapor-phase deposition at 40 °C for 1 h. Second, MicroFil syringe tips (World Precision Instruments, Sarasota, FL) were used to fill nanopipettes with 1 mM solutions of 3-maleimidobenzoic acid *N*-hydroxysuccinimide ester (MBS) dissolved in a 1:9 (v/v) mixture of dimethyl sulfoxide and PBS for 1 h. The MBS crosslinks the amine-terminated silanes to thiolated DNA aptamers. As the third step, aptamers were prepared for functionalization by reducing the disulfide bonds using 50-fold excess tris(2-carboxyethyl) phosphine (TCEP) relative to DNA aptamer concentration (100 μM) at room temperature for 1h.

The aptamers were then diluted to 5 μM in 1x PBS and cleaned with Zeba™ spin desalting columns (7K MWCO, 0.5 mL, ThermoFisher Scientific AG, Reinach, Switzerland). Aptamer solutions were desalted to remove unreacted TCEP, which has been shown to be reactive towards maleimides resulting in byproducts, likely leading to lower coupling yields.[39] Aptamers were then denatured at 95 °C for 5 min then renatured by cooling to room temperature before surface attachment. Nanopipettes were rinsed twice with deionized water using MicroFil tips and then incubated in the aptamer solution for 2 h. Any remaining aptamer solution was rinsed out by PBS three times prior to experimental use.

Sensing measurements *via* aptamer-modified nanopipettes. The current was measured between two Ag/AgCl quasi-reference counter electrodes, one inside the nanopipette and another in the bulk solution, with a custom-built high gain current amplifier. Data recording was performed using a custom written LabVIEW interface (2017, National Instruments), based on WEC-SPM package provided by Warwick Electrochemistry and Interfaces Group, led by Prof. Unwin. Data was collected using an FPGA card PCIe-7852R (National Instruments). The current magnitudes and potentials reported in the manuscript

2

are denoted with respect to the electrode in the solution bulk. Cyclic voltammograms were acquired by sweeping voltage at 0.05 V s^{-1} voltage sweep rate.

Quartz Crystal Microbalance with Dissipation Monitoring (QCM-D). Measurements were performed using the Q-Sense E4 (Biolin Scientific) equipped with four flow modules. The resonance frequency, f, and the energy dissipation of the quartz crystal, D, were measured at the fundamental resonance frequency (5 MHz) as well as the 3rd, 5th, 7th, and 9th overtones. Normalized frequency and dissipation shifts post baseline subtraction in PBS are presented. Aptamer-target binding experiments were conducted in a continuous flow of PBS buffer at a flow rate of 50 µL/min by using an IPC series 4-channel microprocessor controlled dispensing pump from Cole-Parmer GmbH (Wertheim, Germany). The temperature of the QCM-D platform was stabilized at 25 °C and buffers were degassed prior to use to avoid bubble formation.

The QCM-D sensors with Au metallization and SiO$_2$ coating (5 MHz, 14 mm diameter) were purchased from MicroVacuum Ltd. (Budapest, Hungary). Prior to use, the chips were exposed to UV-ozone treatment for 10 min and then immersed sequentially in acetone, isopropanol, then deionized water, and sonicated in each for 3 min. The surfaces were dried under nitrogen before chemical vapor deposition of amine- and methyl-terminated silanes in a 1:9 solution ratio. The chips were then mounted in the QCM-D flow chamber with PBS as the running buffer. The chips were first incubated in MBS for 30 min and then after excessive rinsing with PBS in the flow chamber, exposed to aptamer solution (5 µM in PBS) that was reduced by TCEP and heat-treated prior (following the same protocol as the nanopipette aptamer functionalization, *vide supra*) and incubated until a stable signal was reached after rigorous rinsing in PBS to remove any non-specific surface adsorption. Upon confirming assembly of the aptamer on the surface of the quartz crystal, the analyte (100 µM serotonin) was exposed to the surface. After equilibrium binding was reached, the flow chamber was flushed with PBS to demonstrate reversible binding. To demonstrate sequence specificity, a control DNA sequence was also assembled and tested in a parallel chamber in the QCM-D.

Electrochemical impedance spectroscopy. Gold QCM chips with Au coatings and Cr adhesive layers (14 mm diameter) purchased from MicroVacuum Ltd. (Budapest, Hungary) were cleaned with the same protocol as QCM-D measurements. Subsequently, the Au surface was incubated in aptamer solution (5 µM in PBS) that was reduced by TCEP and heat-treated prior overnight. The following day, the surface was triple washed in deionized water then incubated in 2 mM of 6-mercapto-1-hexanol (MCH) for 30 min to passivate the surface. Nonspecific interactions between gold electrodes and DNA as well as other analytes have been minimized by filling exposed areas with short hydrophilic thiols such as MCH.[40–43] Post MCH assembly, the aptamer-functionalized surfaces were rigorously washed in deionized water.

Electrochemical impedance spectroscopy measurements were performed using the Autolab potentiostat/galvanostat (PGSTAT302N) with a FRA32 module for impedance analysis with the NOVA 2.1 software from Metrohm (Herisau, Switzerland). A three-electrode system was set up with the Au surface serving as the working electrode. A
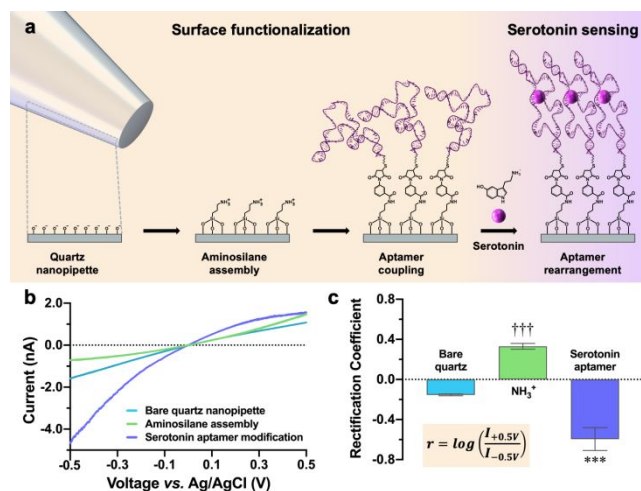

Figure 2. Serotonin aptamer functionalization to quartz nanopipettes and serotonin sensing in PBS. (a) Schematic of the functionalization procedure. A layer of aminosilanes is assembled *via* vapor phase deposition on quartz nanopipette walls. Amine groups (NH$_3^+$) are subsequently covalently coupled to thiolated serotonin aptamers. Upon exposure to serotonin target, aptamers undergo conformational rearrangement, altering the ionic flux through the nanopipette. This schematic is an idealized representation of the sequential surface chemistry inside the nanopipette. **(b)** Representative voltammograms tracking the surface functionalization process show a surface charge dependent rectification of the ion current. **(c)** Rectification coefficients calculated from the current-voltage curves correlate to the surface charge of each functionalization step. While the bare quartz shows a negative rectification, aminosilane-functionalized nanopipettes show a positive rectification. A large negative rectification ratio is observed upon aptamer binding due to coupling of the highly negatively charged oligonucleotides to the quartz surface. Error bars represent standard errors of the mean with $N = 3$ nanopipettes. Group means were significantly different [F(2,6) = 166; ***P <0.001]; ***P < 0.001 *vs.* bare and aminosilane-functionalized nanopipettes; †††P < 0.001 *vs.* bare or aptamer-modified nanopipettes.

polydimethylsiloxane cup was sealed on the surface of the gold surface to confine the liquid and the Ag/AgCl reference electrode and Pt wire as the counter electrode were placed in the solution. Potassium hexacyanoferrate (III) was added to the solution at 2 mM concentration for each measurement. The impedance was measured from 0.01-10^5 Hz with 7 logarithmic spaced frequencies per decade. A sinusoidal alternating voltage with an amplitude of 10 mV was applied.

Statistics. All statistics were carried out using GraphPad Prism (GraphPad Software Inc., San Diego). Data are reported as means ± standard errors of the means with probabilities $P<0.05$ considered statistically significant. Comparative data was evaluated by one-way analysis of variance followed by Tukey's multiple group comparisons. Concentration-dependent responses were fit to the Langmuir isotherm where the Hill slope was assumed to be 1.0 for mass action binding of one serotonin molecule to one recognition site (aptamer).

RESULTS AND DISCUSSION

To transform nanopipettes into serotonin-specific sensors, we functionalized the nanopore surfaces with artificial recognition

elements termed aptamers, which are short single-stranded oligonucleotides that have been designed and selected *in vitro* to bind to targets of interest (Figure 2a).[44–48] Amine-terminated silanes were first assembled *via* chemical vapor deposition forming robust silane layers,[49,50] and coupled to thiolated aptamers *via* thiol-maleimide click chemistry.[38] The serotonin-specific aptamer has been previously demonstrated to undergo significant conformational rearrangements in three-dimensional space upon serotonin recognition in complex environments.[38] Thus, we hypothesized that serotonin aptamers chemically functionalized to nanopipette walls would gate ionic flux by altering local charge densities, and together with the ICR effect, modulate the current response upon serotonin recognition.

The functionalization process was tracked as a function of the change in ICR characteristics in phosphate buffered saline (PBS) to validate aptamer assembly on the surface of nanopipettes (Figure 2b). The ICR magnitude can be represented quantitatively as the rectification ratio (r), expressed as the logarithmic ratio of the current response at a specific potential relative to the current at a potential of equal magnitude but opposite polarity (Figure 2c). Aminosilane (amino groups, $pK_a = 9.6$)[51] functionalization of the bare quartz nanopipette surface (silanol groups, $pK_a \sim 5.6$)[52] alters the rectification ratio from approximately -0.2 to +0.3, and then to -0.8 upon modification with serotonin aptamers (phosphates in nucleic acids, $pK_a \sim 1$).[53] Serotonin aptamer functionalization was tuned by altering both the nanopipette pore size and the surface density of aptamers in the nanopipettes (Figures S1 and S2 Supporting Information).

Upon validation of aptamer functionalization inside the nanopipette, the sensors were tested first in physiological buffer (PBS) for serotonin detection. The initial current-voltage range of the aptamer-modified sensors in PBS was a way to verify effective aptamer functionalization. The baseline current variation in the current-voltage characteristics observed between individual aptamer-modified nanopipettes in PBS is shown in Figure S3a in the Supporting Information. Addition of serotonin at a saturated concentration (100 μM) based on the previously reported binding affinity of the serotonin aptamer ($K_d = 30$ nM),[38] resulted in a measurable change in current response from the baseline current in PBS, with an increase of ~30% at +0.5 V (Figure 3a).

We next interrogated the serotonin aptamer-modified nanopipette selectivity, stability, and sensing capability in neurobasal medium (NBM), the complex environment in which *in vitro* neurons are typically cultured.[54] This medium contains 17 amino acids in high μM concentrations including *L*-tryptophan, a serotonin precursor, in addition to other small molecules and proteins that sustain neural growth. Variability of baseline current between different nanopipettes tested in NBM is shown in Figure S3b in the Supporting Information.

To interrogate the selectivity of serotonin aptamer-modified nanopipettes towards similarly structured neurochemicals in addition to *L*-tryptophan in NBM, we exposed the nanopipettes to high concentrations (100 μM) of the serotonin precursor, *L*-5-hydroxytryptophan (*L*-5-HTP) and the serotonin metabolite, 5-hydroxyindoleacetic acid (5-HIAA) in real time (Figure 3b). Despite comparable molecular structures, negligible perturbations were observed for the nonspecific molecules while a significant increase in current was observed
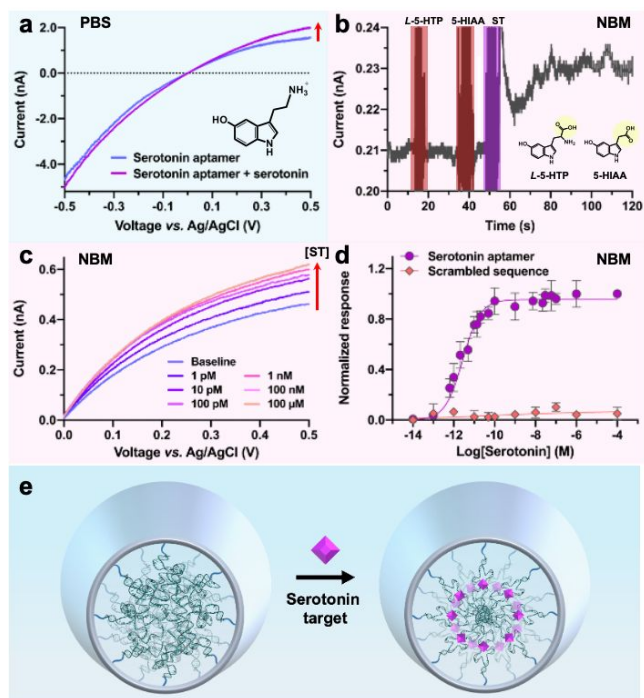

Figure 3. Specificity and selectivity of serotonin-modified nanopipettes. (**a**) Representative voltammograms ($N = 6$) of serotonin aptamer-functionalized nanopipettes before and after exposure to the target serotonin (100 μM) in phosphate-buffered saline (PBS). (**b**) Real-time current measurement in neurobasal medium (NBM) demonstrating the selectivity of serotonin aptamer-modified nanopipettes *versus* similarly structured molecules *L*-5-hydroxytryptophan (*L*-5-HTP) and 5-hydroxyindoleacetic acid (5-HIAA) measured at +0.5 V. While 100 μM concentrations of nonspecific molecules caused negligible changes in current, low concentrations of serotonin (ST; 1 pM) caused a measurable current increase. (**c**) Representative voltammograms of the concentration-specific response of aptamer-modified nanopipettes to serotonin in NBM *via* sequential addition of serotonin from 10 fM to 100 μM. (**d**) From these voltammograms, calibration curves were obtained by normalizing the changes from baseline where no serotonin is present at +0.5 V. Scrambled sequence controls were conducted in parallel and demonstrated minimal response. Error bars represent standard errors of the mean with $N = 6$ nanopipettes per concentration for the serotonin aptamer and $N = 2$ for the scrambled sequence control. (**e**) Schematic for hypothesized mechanism whereby aptamer conformational change upon serotonin binding alters the nanopore conductivity.

upon addition of orders of magnitude lower concentration (1 pM) of the correct target.

Serotonin concentration dependence was interrogated in NBM (Figure 3c) and a dose response curve was obtained using the change in current from baseline to demonstrate the capability of sensing serotonin concentrations in complex environments (Figure 3d). To avoid the variation between different sensors, the signals were normalized to the response in the medium without target molecules. As shown, the current response of nanopipettes was lower in NBM compared to PBS due to the lower ionic content resulting in fewer charge carriers (137 mM NaCl in PBS *vs.* 52 mM NaCl in NBM). To interrogate sequence specificity, a scrambled sequence where the same number of each nucleobase was conserved, but their

order scrambled to alter the recognition behavior, was designed. Measurements with a scrambled sequence conducted in the same experimental procedure yielded negligible responses to serotonin at all concentrations tested.

While the binding affinity of the serotonin aptamer was previously found to be 30 nM in solution *via* fluorescence quenching measurements,[38] aptamer-modified nanopipettes achieved higher sensitivity allowing measurements in the pM range (Figure 3d). Unlike conventional equilibrium sensors where the detection range is limited by the recognition element K_d, the nanopipettes act more like affinity columns or lateral flow assays that operate out of equilibrium. The nanoconfinement in the nanopipette increases the local concentration of both target molecules and aptamers, increasing the frequency of rebinding events,[55] therefore allowing detection of lower concentrations than what is possible with equilibrium assays.[56,57]

Nevertheless, these results demonstrate the specificity and selectivity of serotonin aptamer-modified nanopipettes in complex environments. Further, aptamer-modified nanopipettes remained stable in the NBM for at least 4 h compared to unmodified quartz nanopipettes that typically clog immediately (Figure S4 in the Supporting Information). This stability likely arises from the aptamer modification that occludes the nanopore, preventing the entry of proteins and other macromolecules.

In addition to demonstrating the sensing capability of these aptamer-modified nanopipettes in real matrices, we also hypothesize a novel mechanistic model for aptamer-modified nanopipette sensing: aptamers undergo complex secondary structure rearrangements that result in changes in permeability and the charge distribution within the aptamer layer that both affect ionic flow (Figure 3e). The degree of blocking of ion flux by aptamers at the tip as well as the density of fixed charges on the backbone of the aptamer molecule are dependent on its conformation. Thus, target-induced conformational change seems to be the reason for the observed significant change in the ionic transport across the nanopore.

Previous reports on signal transduction resulting from target recognition by aptamer-functionalized synthetic nanopores have proposed mechanistic hypotheses such as orifice blockage upon target capture[58,59] or alterations in the surface charge due to aptamer-target binding.[60,61] On the contrary to these reports, binding of the small-molecule serotonin, with a single positive charge (at pH 7.4), is unlikely to cause a significant change in surface charge relative to the highly negatively charged aptamers. Therefore, the ICR response is likely to be dictated by the spatial charge redistribution of the aptamer layer itself.

To correlate this hypothesis to the specific conformational changes of the serotonin aptamer upon target recognition, we employed several surface characterization techniques such as quartz crystal microbalance with dissipation monitoring (QCM-D) and electrochemical impedance spectroscopy (EIS). In QCM-D, changes in the resonance frequency (Δf) of a quartz sensor are related to the change in coupled mass at the sensor surface, and the variations in dissipation energy (ΔD) are correlated to the viscoelastic properties of the oscillating mass. This method has been previously used to characterize aptamer-small-molecule target interactions.[62–64] For example, Osypova *et al.* exploited aptamer conformational change as a way to amplify the binding signal of the small molecule *L-*
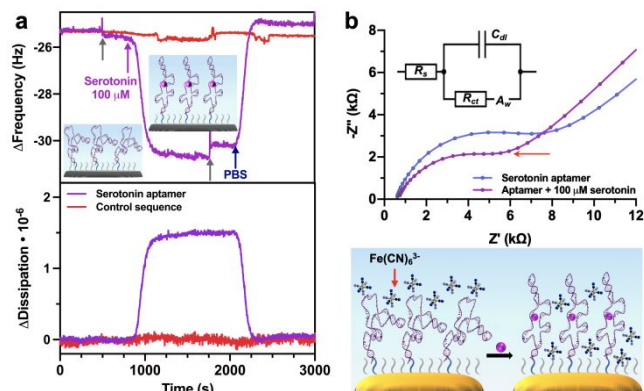

Figure 4. Characterization of serotonin aptamer-modified surfaces. (**a**) The decreasing frequency and increasing dissipation values upon serotonin target addition indicate an increase of aptamer layer thickness in quartz crystal microbalance with dissipation monitoring measurements. Switching to phosphate buffered saline (PBS) demonstrates reversible binding. Grey arrows indicate when the solution was switched while subsequent colored arrows indicate when the solution reached the sensor surface. A control scrambled sequence measured in parallel, resulted in minimal signal change upon equimolar serotonin addition. (**b**) Electrochemical impedance spectroscopy showed changes in the charge transfer resistance (R_{ct}) of a redox reporter, ferricyanide ($Fe(CN)_6^{3-}$) upon aptamer-target complex formation. The Nyquist plots were fitted to a Randles circuit. The R_{ct} decreased upon target addition, suggesting improved penetration of the $Fe(CN)_6^{3-}$ to reach the surface.

tyrosinamide, where the aptamer backbone rearrangement induces the displacement of water that is acoustically coupled to the sensing layer.[64]

Upon validating the assembly of an aptamer monolayer of ~5 nm in thickness (Figure S5a Supporting Information), the sensor surface was exposed to the target serotonin and a decrease in the frequency by ~ 5 Hz was observed and an increase in dissipation of ~1.5 x 10⁻⁶ (Figure 4a). After a rinsing step with PBS, the signal returned to its initial value, indicating the reversibility of the recognition process. Observation of reversible binding was possible in the QCM-D due to fluidics integrated on its planar sensors that enabled rigorous rinsing at the surface to remove targets released by aptamers. However, removal of released targets in the confined nanoscale orifice inside nanopipettes is not as straightforward and is still under investigation for optimal and reproducible sensor regeneration.

In contrast to the serotonin-specific aptamer results, a control scrambled sequence measured in parallel, showed a negligible response upon exposure to serotonin. Quantitative analysis of the QCM-D data through viscoelastic modeling correlated the frequency and dissipation shifts to an *increase* in aptamer monolayer thickness by approximately 1.2 nm (Figure S5b, Table S1 Supporting Information).

Alternatively, to interrogate the surface accessibility to ions driven by the serotonin aptamer undergoing conformational rearrangement upon target capture, we conducted electrochemical impedance spectroscopy (EIS) measurements. A redox reporter ferricyanide ($Fe(CN)_6$)³⁻ was added to observe changes in the electron transfer at the solution-surface interface upon serotonin addition. The Faradaic impedance spectra presented as Nyquist plots in Figure 4b show that upon serotonin incubation, the electron transfer resistance (R_{ct};

5

semicircle diameter) *decreases*, suggesting that the aptamer backbone rearrangement facilitates the access of $(Fe(CN)_6)^{3-}$ molecules to the electrode. At the same time, only minimal changes in solution resistance (R_s), double layer capacitance (C_{dl}) and the Warburg impedance (A_w), which represents the diffusion of all ions to the electrode surface, were observed (Table S2 Supporting Information).

Both QCM-D and EIS measurements support the hypothesis that conformational change of aptamers occurring predominantly at the nanopipette tip, is responsible for signal transduction. The nanopipette tip is the most sensitive region for sensing where 50% of the electrical resistance of the sensor is confined within the *ca*. 30 nm-long tip section (Figures S6 and S7 Supporting Information). However, the unusual change of the current-voltage curve upon target addition, led us to believe that the sensing mechanism is not as simple as aptamer-target binding resulting in an open *versus* closed nanopore.

Specifically, two phenomena are observed: (i) change in the permeability of the aptamer layer (*e.g.* a decrease of the resistance from 188 to 158 MΩ (*ca*. 16%) as observed for data in Figure 3a at low bias magnitudes where ICR is minimal) and (ii) variation of the charge density due to "dilution" charge in a 24% thicker layer of the aptamer upon interaction with serotonin (6.2 nm vs. 5 nm). Both smaller charge density and higher permeability lead to a current increase at positive bias, while at negative bias these factors can cancel each other out leading to a different variation of the measured ion flux. In some cases, the current at negative biases varied slightly, like shown in Figure 3a, however, with no evident trend in directionality of change or concentration dependence. Hence, current at negative voltage polarity could not be used for quantification of serotonin. On the contrary, ion current magnitudes at positive biases were directly related to serotonin content (Figure 3c). Despite the difficulty in precise quantification of these ion transport phenomena (also because the model neglects the contribution from electroosmotic flow, EOF), our qualitative finite element method model supports these observations (Figure S8 Supporting Information).

Alternatively, the unusual change of the voltametric nanopipette response to serotonin presence can be related to asymmetric mass-transport of the analyte. At negative pipette bias, serotonin is driven inwards by the electric field that can reach 67 MV/m at the orifice already at -0.1 V. This field may be strong enough to pull serotonin species rapidly through the nanopore so that the retention time is shorter than characteristic time for aptamer-target recognition (typically on the order of seconds, Figure 4a). In addition to electrophoretic flux, serotonin can be driven by EOF, which has the same direction, assisting in the accumulation of analyte inside the nanopipette. On the contrary, at positive biases, serotonin species encounter a large electrophoretic force (electric field spike at the border between the aptamer layer and bulk solution), which prevents the analyte from a quick escape from the pipette tip (Figure S9 Supporting Information). This phenomenon may potentially lead to a longer retention of serotonin at the orifice, resulting in changes in both ICR and permeability.

Our hypothesis is supported by transient pulse measurements, where a decay in the current magnitude is observed at positive bias in the presence of the serotonin aptamers *versus* bare unmodified quartz nanopipettes with much smaller ion flux variation at negative bias (Figure S10a Supporting Information). Further, addition of serotonin changes the shape of the decay curve at positive bias while minimal changes are observed at negative voltages (Figure S10b Supporting Information). Since the flux of serotonin itself does not contribute to the total magnitude of the overall ion current, the observed current variations highlight the changes in aptamer layer upon target binding.

While the exact reason for an asymmetric effect on the current-voltage characteristic of the nanopipette sensor remains unclear, our collective observations from ICR, QCM-D, and EIS support our mechanistic model of small-molecule sensing *via* aptamer-modified nanopipettes, which is a complex nanoscale phenomenon where aptamer conformational change within the confined orifice of nanopipettes is the principal factor for serotonin detection.

CONCLUSIONS

In this work, we developed a sensitive and selective analytical platform for quantification of serotonin using chemically modified glass nanopores with *ca*. 10 nm openings. The sensitivity and selectivity of the response to serotonin analytes is based on specific chemical interactions between serotonin aptamers covalently bound to the glass walls and target species that cause changes in physicochemical properties at the nanopipette tip. The nanoscale confinement of the pore plays an important role for signal transduction: we demonstrate that the target-induced conformation change of aptamer molecules leads to local changes in pore permeability and charge arrangement, resulting in changes of ion flow through the pore due to the phenomenon of ion current rectification. We further validated these observations using numerical modeling that qualitatively corroborate theoretical and experimental rectification responses. Complementary data from surface-sensitive techniques, such as electrochemical impedance spectroscopy and quartz crystal microbalance measurements with dissipation monitoring support our mechanistic studies.

Our aptamer-modified nanopipette sensors demonstrated specific and selective responses to serotonin for real-world sensing applications. The performance of the analytical platform was validated in the presence of high concentrations of interferents with similar chemical structure in complex media, such as neurobasal medium. Sensors remained robust for extended periods of time (>4 h) compared to unmodified nanopipettes that clog within minutes.

To this end, aptamer nanopipette sensors are promising for future investigations for interrogating neurochemical flux in close proximity to synapses of neural networks *in situ*. It is particularly attractive to combine its functional sensing capacity with precise positioning and imaging using advanced electrochemical techniques, such as scanning ion conductance[29] or scanning nanopore microscopes[26] for monitoring neurochemical processes occurring at cellular interfaces with nanoscale resolution. When coupled to advanced high-speed scanning technologies capable of recording multiple image frames in a matter of seconds,[27,28,65] this platform can provide a plethora of new information and potentially overcome the difficulties related to sensitivity (low analyte concentration) and selectivity typical for other (electrode-based) amperometric electrochemical techniques.

ASSOCIATED CONTENT

Supporting Information

The Supporting Information is available free of charge on the ACS Publications website.

Sensor characterization (Figures S1 and S2); Baseline current variability for aptamer-modified nanopipettes (Figure S3); Aptamer-functionalized nanopipette stability in complex media (Figure S4); Surface characterization of aptamer-modified surfaces (Figure S5); Numerical simulations (Figures S6-S9); Transient pulse measurements (Figure S10); Table S1: Values of the fitted parameters for QCM-D measurements; Table S2: Values of the equivalent circuit parameters of fitting Nyquist curves; Table S3: Boundary conditions of the numerical model and specific parameters in model domains (PDF).

AUTHOR INFORMATION

Corresponding Authors

*Dmitry Momotenko – *Laboratory of Biosensors and Bioelectronics, Institute for Biomedical Engineering, ETH Zürich, CH-8092, Switzerland;* Email: momotenko@biomed.ee.ethz.ch

*Janos Vörös – *Laboratory of Biosensors and Bioelectronics, Institute for Biomedical Engineering, ETH Zürich, CH-8092, Switzerland;* Email: janos.voros@biomed.ee.ethz.ch

Present Address

†**Csaba Forró** – *Department of Chemistry, Stanford University, Stanford, CA 94305, USA*

Notes

The authors declare no competing financial interest.

REFERENCES

(1) Hagena, H.; Manahan-Vaughan, D. MGlu5 acts as a switch for opposing forms of synaptic plasticity at mossy fiber–CA3 and commissural associational–CA3 synapses. *J. Neurosci.* **2015**, *35*, 4999–5006.

(2) Lovinger, D. M. Neurotransmitter roles in synaptic modulation, plasticity and learning in the dorsal striatum. *Neuropharmacology* **2010**, *58*, 951–961.

(3) Pedigo, N. W. Neurotransmitter receptor plasticity in aging. *Life Sci.* **1994**, *55*, 1985–1991.

(4) Lesch, K. P.; Waider, J. Serotonin in the modulation of neural plasticity and networks: implications for neurodevelopmental disorders. *Neuron* **2012**, *76*, 175–191.

(5) Cavaccini, A.; Gritti, M.; Giorgi, A.; Locarno, A.; Heck, N.; Migliarini, S.; Bertero, A.; Mereu, M.; Margiani, G.; Trusel, M.; Catelani, T.; Marotta, R.; De Luca, M. A.; Caboche, J.; Gozzi, A.; Pasqualetti, M.; Tonini, R. Serotonergic signaling controls input-specific synaptic plasticity at striatal circuits. *Neuron* **2018**, *98*, 801–816.

(6) Liu, Y.; Zhang, J.; Xu, X.; Zhao, M. K.; Andrews, A. M.; Weber, S. G. Capillary ultrahigh performance liquid chromatography with elevated temperature for sub-one minute separations of basal serotonin in submicroliter brain microdialysate samples. *Anal. Chem.* **2010**, *82*, 9611–9616.

(7) Zhang, J.; Liu, Y.; Jaquins-Gerstl, A.; Shu, Z.; Michael, A. C.; Weber, S. G. Optimization for speed and sensitivity in capillary high performance liquid chromatography: the importance of column diameter in online monitoring of serotonin by microdialysis. *J. Chromatogr. A* **2012**, *1251*, 54–62.

(8) Yang, H.; Thompson, A. B.; McIntosh, B. J.; Altieri, S. C.; Andrews, A. M. Physiologically relevant changes in serotonin resolved by fast microdialysis. *ACS Chem. Neurosci.* **2013**, *4*, 790–798.

(9) Dankoski, E. C.; Mark Wightman, R. Monitoring serotonin signaling on a subsecond time scale. *Front. Integr. Neurosci.* **2013**, *7*, 1–13.

(10) Travis, E. R.; Wang, Y. M.; Michael, D. J.; Caron, M. G.; Wightman, R. M. Differential quantal release of histamine and 5-hydroxytryptamine from mast cells of vesicular monoamine transporter 2 knockout mice. *Proc. Natl. Acad. Sci. U. S. A.* **2000**, *97*, 162–167.

(11) Jackson, B. P.; Dietz, S. M.; Wightman, R. M. Fast-scan cyclic voltammetry of 5-hydroxytryptamine. *Anal. Chem.* **1995**, *67*, 1115–1120.

(12) Nakatsuka, N.; Andrews, A. M. A. M. Differentiating siblings: the case of dopamine and norepinephrine. *ACS Chem. Neurosci.* **2017**, *8*, 218–220.

(13) Puthongkham, P.; Venton, B. J. Recent advances in fast-scan cyclic voltammetry. *Analyst* **2020**, *145*, 1087–1102.

(14) Sharma, S.; Singh, N.; Tomar, V.; Chandra, R. A review on electrochemical detection of serotonin based on surface modified electrodes. *Biosens. Bioelectron.* **2018**, *107*, 76–93.

(15) Patel, B. A. Continuous amperometric detection of co-released serotonin and melatonin from the mucosa in the ileum. *Analyst* **2008**, *133*, 516–524.

(16) Jeong, S.; Yang, D.; Beyene, A. G.; Del Bonis-O'Donnell, J. T.; Gest, A. M. M.; Navarro, N.; Sun, X.; Landry, M. P. High-throughput evolution of near-infrared serotonin nanosensors. *Sci. Adv.* **2019**, *5*, 1–12.

(17) Hai, A.; Cai, L. X.; Lee, T.; Lelyveld, V. S.; Jasanoff, A. Molecular fMRI of serotonin transport. *Neuron* **2016**, *92*, 754–765.

(18) Forró, C.; Thompson-Steckel, G.; Weaver, S.; Weydert, S.; Ihle, S.; Dermutz, H.; Aebersold, M. J.; Pilz, R.; Demkó, L.; Vörös, J. Modular microstructure design to build neuronal networks of defined functional connectivity. *Biosens. Bioelectron.* **2018**, *122*, 75–87.

(19) Weydert, S.; Girardin, S.; Cui, X.; Zürcher, S.; Peter, T.; Wirz, R.; Sterner, O.; Stauffer, F.; Aebersold, M. J.; Tanner, S.; Thompson-Steckel, G.; Forró, C.; Tosatti, S.; Vörös, J. A versatile protein and cell patterning method suitable for long-term neural cultures. *Langmuir* **2019**, *35*, 2966–2975.

(20) Alivisatos, A. P.; Andrews, A. M.; Boyden, E. S.; Chun, M.; Church, G. M.; Deisseroth, K.; Donoghue, J. P.; Fraser, S. E.; Lippincott-Schwartz, J.; Looger, L. L.; Masmanidis, S.; McEuen, P. L.; Nurmikko, A. V.; Park, H.; Peterka, D. S.; Reid, C.; Roukes, M. L.; Scherer, A.; Schnitzer, M.; Sejnowski, T. J.; Shepard, K. L.; Tsao, D.; Turrigiano, G.; Weiss, P. S.; Xu, C.; Yuste, R.; Zhuang, X. Nanotools for neuroscience and brain activity mapping. *ACS Nano* **2013**, *7*, 1850–1866.

(21) Fan, R.; Karnik, R.; Yue, M.; Li, D.; Majumdar, A.; Yang, P. DNA translocation in inorganic nanotubes. *Nano Lett.* **2005**, *5*, 1633–1637.

(22) Gong, X.; Patil, A. V.; Ivanov, A. P.; Kong, Q.; Gibb, T.; Dogan, F.; Demello, A. J.; Edel, J. B. Label-free in-flow detection of single DNA molecules using glass nanopipettes. *Anal. Chem.* **2014**, *86*, 835–841.

(23) Heins, E. A.; Siwy, Z. S.; Baker, L. A.; Martin, C. R. Detecting single porphyrin molecules in a conically shaped synthetic nanopore. *Nano Lett.* **2005**, *5*, 1824–1829.

(24) Kasianowicz, J. J.; Brandin, E.; Branton, D.; Deamer, D. W. Characterization of individual polynucleotide molecules using a

7

membrane channel. *Proc. Natl. Acad. Sci. U. S. A.* **1996**, *93*, 13770–13773.

(25) Meller, A.; Nivon, L.; Brandin, E.; Golovchenko, J.; Branton, D. Rapid nanopore discrimination between single polynucleotide molecules. *Proc. Natl. Acad. Sci. U. S. A.* **2000**, *97*, 1079–1084.

(26) Aramesh, M.; Forró, C.; Dorwling-Carter, L.; Lüchtefeld, I.; Schlotter, T.; Ihle, S. J.; Shorubalko, I.; Hosseini, V.; Momotenko, D.; Zambelli, T.; Klotzsch, E.; Vörös, J. Localized detection of ions and biomolecules with a force-controlled scanning nanopore microscope. *Nat. Nanotechnol.* **2019**, *14*, 791–798.

(27) Ida, H.; Takahashi, Y.; Kumatani, A.; Shiku, H.; Matsue, T. High speed scanning ion conductance microscopy for quantitative analysis of nanoscale dynamics of microvilli. *Anal. Chem.* **2017**, *89*, 6015–6020.

(28) Momotenko, D.; McKelvey, K.; Kang, M.; Meloni, G. N.; Unwin, P. R. Simultaneous interfacial reactivity and topography mapping with scanning ion conductance microscopy. *Anal. Chem.* **2016**, *88*, 2838–2846.

(29) Hansma, P. K.; Drake, B.; Marti, O.; Gould, S. A. C.; Prater, C. B. The scanning ion-conductance microscope. *Science* **1989**, *243*, 641–643.

(30) Actis, P.; Rogers, A.; Nivala, J.; Vilozny, B.; Seger, R. A.; Jejelowo, O.; Pourmand, N. Reversible thrombin detection by aptamer functionalized sting sensors. *Biosens. Bioelectron.* **2011**, *26*, 4503–4507.

(31) Lin, D. H.; Lin, C. Y.; Tseng, S.; Hsu, J. P. Influence of electroosmotic flow on the ionic current rectification in a pH-regulated, conical nanopore. *Nanoscale* **2015**, *7*, 14023–14031.

(32) Wei, C.; Bard, A. J.; Feldberg, S. W. Current rectification at quartz nanopipet electrodes. *Anal. Chem.* **1997**, *69*, 4627–4633.

(33) Hsu, J. P.; Yang, S. T.; Lin, C. Y.; Tseng, S. Ionic current rectification in a conical nanopore: influences of electroosmotic flow and type of salt. *J. Phys. Chem. C* **2017**, *121*, 4576–4582.

(34) Momotenko, D.; Girault, H. H. Scan-rate-dependent ion current rectification and rectification inversion in charged conical nanopores. *J. Am. Chem. Soc.* **2011**, *133*, 14496–14499.

(35) Kubeil, C.; Bund, A. The role of nanopore geometry for the rectification of ionic currents. *J. Phys. Chem. C* **2011**, *115*, 7866–7873.

(36) Momotenko, D.; Cortés-Salazar, F.; Josserand, J.; Liu, S.; Shao, Y.; Girault, H. H. Ion current rectification and rectification inversion in conical nanopores: a perm-selective view. *Phys. Chem. Chem. Phys.* **2011**, *13*, 5430–5440.

(37) Zuker, M. Mfold web server for nucleic acid folding and hybridization prediction. *Nucleic Acids Res.* **2003**, *31*, 3406–3415.

(38) Nakatsuka, N.; Yang, K.-A.; Abendroth, J. M.; Cheung, K. M.; Xu, X.; Yang, H.; Zhao, C.; Zhu, B.; Rim, Y. S.; Yang, Y.; Weiss, P. S.; Stojanović, M. N.; Andrews, A. M. Aptamer–field-effect transistors overcome debye length limitations for small-molecule sensing. *Science* **2018**, *362*, 319–324.

(39) Kantner, T.; Watts, A. G. Characterization of reactions between water-soluble trialkylphosphines and thiol alkylating reagents: implications for protein-conjugation reactions. *Bioconjug. Chem.* **2016**, *27*, 2400–2406.

(40) Kafka, J.; Pänke, O.; Abendroth, B.; Lisdat, F. A label-free DNA sensor based on impedance spectroscopy. *Electrochim. Acta* **2008**, *53*, 7467–7474.

(41) Riedel, M.; Kartchemnik, J.; Schöning, M. J.; Lisdat, F. Impedimetric DNA detection-steps forward to sensorial application. *Anal. Chem.* **2014**, *86*, 7867–7874.

(42) Tersch, C.; Lisdat, F. Label-free detection of protein-DNA interactions using electrochemical impedance spectroscopy. *Electrochim. Acta* **2011**, *56*, 7673–7679.

(43) Witte, C.; Lisdat, F. Direct detection of DNA and DNA-ligand interaction by impedance spectroscopy. *Electroanalysis* **2011**, *23*, 339–346.

(44) Ellington, A. D.; Szostak, J. W. *In vitro* selection of RNA molecules that bind specific ligands. *Nature* **1990**, *346*, 818–822.

(45) Tuerk, C.; Gold, L. Systematic evolution of ligands by exponential enrichment: RNA ligands to bacteriophage T4 DNA polymerase. *Science* **1990**, *249*, 505–510.

(46) Baker, M. Reproducibility crisis: blame it on the antibodies. *Nature* **2015**, *521*, 274–276.

(47) Hermann, T.; Patel, D. J. Adaptive recognition by nucleic acid aptamers. *Science* **2000**, *287*, 820–825.

(48) Ricci, F.; Vallée-Bélisle, A.; Simon, A. J.; Porchetta, A.; Plaxco, K. W. Using nature's "tricks" to rationally tune the binding properties of biomolecular receptors. *Acc. Chem. Res.* **2016**, *49*, 1884–1892.

(49) Zhu, M.; Lerum, M. Z.; Chen, W. How to prepare reproducible, homogeneous, and hydrolytically stable aminosilane-derived layers on silica. *Langmuir* **2012**, *28*, 416–423.

(50) Zhang, F.; Sautter, K.; Larsen, A. M.; Findley, D. A.; Davis, R. C.; Samha, H.; Linford, M. R. Chemical vapor deposition of three aminosilanes on silicon dioxide: surface characterization, stability, effects of silane concentration, and cyanine dye adsorption. *Langmuir* **2010**, *26*, 14648–14654.

(51) Pick, C.; Argento, C.; Drazer, G.; Frechette, J. Micropatterned charge heterogeneities *via* vapor deposition of aminosilanes. *Langmuir* **2015**, *31*, 10725–10733.

(52) Behrens, S. H.; Grier, D. G. The charge of glass and silica surfaces. *J. Chem. Phys.* **2001**, *115*, 6716–6721.

(53) Thaplyal, P.; Bevilacqua, P. C. Experimental approaches for measuring pKa's in RNA and DNA. *Methods Enzymol.* **2014**, *549*, 189–219.

(54) Bardy, C.; Van Den Hurk, M.; Eames, T.; Marchand, C.; Hernandez, R. V.; Kellogg, M.; Gorris, M.; Galet, B.; Palomares, V.; Brown, J.; Bang, A. G.; Mertens, J.; Böhnke, L.; Boyer, L.; Simon, S.; Gage, F. H. Neuronal medium that supports basic synaptic functions and activity of human neurons *in vitro*. *Proc. Natl. Acad. Sci. U. S. A.* **2015**, *112*, 2725–2734.

(55) Rajendran, P.; Kaufmann, S.; Vörös, J.; Zenobi-Wong, M.; Demkó, L. Femtomolar oligonucleotide detection by a one-step gold nanoparticle-based assay. *Colloids Surf. B* **2015**.

(56) Freedman, K. J.; Otto, L. M.; Ivanov, A. P.; Barik, A.; Oh, S. H.; Edel, J. B. Nanopore sensing at ultra-low concentrations using single-molecule dielectrophoretic trapping. *Nat. Commun.* **2016**, *7*, 1–9.

(57) Yu, R. J.; Ying, Y. L.; Hu, Y. X.; Gao, R.; Long, Y. T. Label-free monitoring of single molecule immunoreaction with a nanopipette. *Anal. Chem.* **2017**, *89*, 8203–8206.

(58) Abelow, A. E.; Schepelina, O.; White, R. J.; Vallée-Bélisle, A.; Plaxco, K. W.; Zharov, I. Biomimetic glass nanopores employing aptamer gates responsive to a small molecule. *Chem. Commun.* **2010**, *46*, 7984–7986.

(59) Ding, S.; Gao, C.; Gu, L. Q. Capturing single molecules of immunoglobulin and ricin with an aptamer-encoded glass nanopore. *Anal. Chem.* **2009**, *81*, 6649–6655.

(60) Cai, S. L.; Cao, S. H.; Zheng, Y. Bin; Zhao, S.; Yang, J. L.; Li, Y. Q. Surface charge modulated aptasensor in a single glass conical nanopore. *Biosens. Bioelectron.* **2015**, *71*, 37–43.

(61) Cai, S. L.; Zheng, Y. Bin; Cao, S. H.; Cai, X. H.; Li, Y. Q. A conformation and charge co-modulated ultrasensitive biomimetic ion channel. *Chem. Commun.* **2016**, *52*, 12450–12453.

(62) Serrano-Santos, M. B.; Llobet, E.; Özalp, V. C.; Schäfer, T. Characterization of structural changes in aptamer films for controlled release nanodevices. *Chem. Commun.* **2012**, *48*, 10087–10089.

(63) Özalp, V. C. Acoustic quantification of atp using a quartz crystal microbalance with dissipation. *Analyst* **2011**, *136*, 5046–5050.

(64) Osypova, A.; Thakar, D.; Dejeu, J.; Bonnet, H.; Van Der Heyden, A.; Dubacheva, G. V.; Richter, R. P.; Defrancq, E.; Spinelli, N.; Coche-Guérente, L.; Labbé, P. Sensor based on aptamer folding to detect low-molecular weight analytes. *Anal. Chem.* **2015**, *87*, 7566–7574.

(65) Novak, P.; Shevchuk, A.; Ruenraroengsak, P.; Miragoli, M.; Thorley, A. J.; Klenerman, D.; Lab, M. J.; Tetley, T. D.; Gorelik, J.; Korchev, Y. E. Imaging single nanoparticle interactions with human lung cells using fast ion conductance microscopy. *Nano Lett.* **2014**, *14*, 1202–1207.

8

For Table of Contents Only